Journal Pre-proofs

Hydrostatic integrity of the intervertebral disc assessed by MRI

Jonas Widmer, Frédéric Cornaz, Nadja A. Farshad-Amacker, Jess G. Snedeker, med. José Miguel Spirig, Mazda Farshad

PII: S0021-9290(21)00430-9
DOI: https://doi.org/10.1016/j.jbiomech.2021.110661
Reference: BM 110661

To appear in: *Journal of Biomechanics*

Received Date: 6 May 2021
Revised Date: 27 July 2021
Accepted Date: 28 July 2021

Please cite this article as: J. Widmer, F. Cornaz, N.A. Farshad-Amacker, J.G. Snedeker, med. José Miguel Spirig, M. Farshad, Hydrostatic integrity of the intervertebral disc assessed by MRI, *Journal of Biomechanics* (2021), doi: https://doi.org/10.1016/j.jbiomech.2021.110661

Hydrostatic integrity of the intervertebral disc assessed by MRI

Jonas Widmer PhD ETH[1,2], Dr med. Frédéric Cornaz[1,2], PD Dr. med. Nadja A. Farshad-Amacker[3], Prof. Jess G. Snedeker PhD[1,2], Dr. med. José Miguel Spirig[1], Prof. Dr. med Mazda Farshad, MPH[1]

[1] Department of Orthopaedics, Balgrist University Hospital, Zurich, Switzerland
[2] Institute for Biomechanics, ETH Zurich, Zurich, Switzerland
[3] Radiology, Balgrist University Hospital, Zurich, Switzerland

Corresponding author:
Jonas Widmer MSc ETH
Balgrist University Hospital
Department of Orthopaedics, University of Zurich
Institute for Biomechanics, ETH Zurich
Balgrist Campus, Lengghalde 5
CH - 8008 Zurich
Tel +41 44 386 3004
Fax +41 44 386 3009
jonas.widmer@balgrist.ch

Conflict of interest statement
None in relation to the content of this manuscript. No external funding was received.

Ethics
Ethical approval was obtained by the local authorities (BASEC Nr. 2017-00874).

Key Words
Lumbar spine, pressure profilometry, hydrostatic integrity, degeneration, intervertebral disc

Word Count of Manuscript
3039

ABSTRACT

Hydrostatic integrity of the intervertebral disc (IVD) is lost during the process of degeneration. Invasive pressure profilometry (IPP) can quantify it, however, is not applicable for clinical use. We aimed to investigate correlations between IPP and MRI findings to assess non-invasive MRI based methods for prediction of hydrostatic integrity of the intervertebral disc. The pressure profiles of 39 lumbar spinal segments originating from 22 human cadavers were recorded during axial compression in the neutral, the flexed and the extended positions. Disc pressure profiles were measured and mathematically transformed to a novel metric that quantifies pressure profile heterogeneity across the disc. The relationship between pressure profile inhomogeneity ("pressure score") and clinically established magnetic resonance-based classifications systems and demographic parameters was then tested using Spearman correlation tests. Pressure profile inhomogeneities were correlated with IVD degeneration (according to Pfirrmann, rho=0.43, p=0.006), endplate defects (according to Rajasekaran, rho=0.39, p=0.013), segmental degeneration (according to Farshad, rho=0.41, p=0.009) and age (rho=0.32, p=0.049). Modic changes per se did not affect the pressure profiles significantly (p=0.23) and pressure scores did not correlate with BMI (rho= -0.21, p=0.2). Heterogeneity of segmental IVD pressure profiles is a unique measure of disc function. We demonstrate that established clinical methods for MRI characterization of the intervertebral disc, the endplate and overall segmental degeneration all correlate with the hydrostatic integrity of the IVD and can be used for its assessment.

INTRODUCTION

The intervertebral disc (IVD) plays an integral part in spine biomechanics by transmitting high loads whilst providing large flexibility. These characteristics set very high demands on functionality and durability of the tissue, which are provided through a sophisticated interplay of a ligamentous ring, the annulus fibrosus, and the gelatin like core, the nucleus pulposus. The high fluid content of the IVD helps with load damping, allows force transmission and helps distribute compressive loads over the whole disc area, preventing local pressure peaks. In 1992, a pressure transducer in the shape of a

needle was developed to investigate the hydrostatic pressure within the IVD (McNally et al., 1992). Shortly after, a method called pressure profilometry, was introduced to obtain a hydrostatic pressure profile by moving the needle through the IVD (Adams and McNally, 1992). In healthy discs, a largely constant and smooth hydrostatic pressure profile was observed through the nucleus and the largest part of the annulus (Adams and McNally, 1992). In specimens with light degeneration, this uniform pressure profile was observed to become more H-shaped with larger pressure peaks in the annulus and in specimens with more severe degeneration, the profiles became more erratic and spikier, with regions of high-pressure peaks and completely depressurized zones. It was assumed that endplate defects, annulus tears or sclerotic zones prevent fluid dispersion and load distribution (McNally et al., 1996; Przybyla et al., 2006). Regional overload of the highly innervated endplate has been associated with pain (Jackson et al., 1966) and changes in the pressure profile were highly associated with discogenic pain by provocative discography (McNally et al., 1996). Pressure profilometry was therefore suggested as a diagnostic tool to evaluate the hydrostatic integrity of the IVD. However, as iatrogenic generated disc lesions were found to induce cell death and disc degeneration (Gruber et al., 2011), clinical pressure profilometry was discontinued. Since no clear association between the radiologic appearance and the qualitatively evaluated shape of the pressure profiles was reported (McNally et al., 1996), no non-invasive, clinically applicable methods to estimate the pressure profile (or the hydrostatic integrity) are available. However, knowledge about the hydrostatic state of the IVD could be extremely helpful in the clinical setting. Since a clear association between the shape of pressure profiles and the macroscopic appearance of the intervertebral disc was noted (Adams et al., 1996), a systematic analysis of the correlation with established radiologic classification systems could be effective. To this end, a method to quantify the shape of the hydrostatic pressure profile is required. The goal of this study was to create a quantification method for the shape of pressure profiles, to apply this method to the pressure profiles of human cadavers and to evaluate the association with established radiologic grading systems and demographic parameters of the specimens.

MATERIAL AND METHODS

Dissection, preparation and storage

39 spinal segments (8x T12L1, 10x L1L2, 4x L2L3, 9x L3L4, 8x L4L5) arising from 22 fresh frozen cadavers stored at –20 °C until dissection (5 female and 17 male, age: 63-74 years, further information in appendix) were used for this study (Science Care, Phoenix, AZ, USA). Ethical approval was obtained by the local authorities (BASEC Nr. 2017-00874). After thawing, sagittal T2w turbo spin-echo (TSE) dixon images, including water only (repetition time (TR) / echo time (TE) 4000 ms /86 ms; Field of view (FOV) 350 mm; matrix 512 x 512 pixels; echonumbers 1; slice thickness 3mm; flip angle 150; echo train length 17), sagittal T1w TSE (repetition time (TR) / echo time (TE) 750 ms /8.7 ms; Field of view (FOV) 350 mm; matrix 512 x 512 pixels; echonumbers 1; slice thickness 3 mm; flip angle 159; echo train length 4) and axial T2w TSE (repetition time (TR) / echo time (TE) 3620 ms /96 ms; Field of view (FOV) 210 mm; matrix 512 x 512 pixels; echonumbers 1; slice thickness 3 mm; flip angle 15; echo train length 16) were performed on a 3T MRI scanner (Magnetom Prisma, Siemens Medical Solutions, Erlangen, Germany) in order to evaluate IVD-degeneration based on the Pfirrmann classification (Pfirrmann et al., 2001), endplate integrity according to Rajasekaran (Rajasekaran et al., 2008) and segmental degeneration according to Farshad (Farshad-Amacker et al., 2017). Furthermore, the specimens were evaluated for the presence of Modic-changes (Modic et al., 1988). Radiologic evaluation was conducted by an experienced radiologist. The specimens were further checked for bony defects and spinal disease such as ankylosing spondylitis. Careful dissection was performed without harming bony structures, paraspinal ligaments and the intervertebral disc. The IVD was punctured with a 1.6 mm Kirschner wire in the mid-sagittal plane as preparation for the insertion of the pressure needle.

Biomechanical Test Setup

A static biaxial test machine (Zwick/Roell Allroundline 10kN and testXpert III Software, ZwickRoell GmbH & Co. KG, Germany) was used for biomechanical testing. A custom-made testing setup combined with 3D-printed clamps (Cornaz et al., 2020) was used for the fixation of the specimens in

the horizontal position (figure 1A). Axial compression was generated with a horizontally oriented piston (Festo, DSNU-32-80-PPV-A) connected to the x-y-plane, while flexion-extension loading was generated with the torsional motor of the test machine. A linear stepper motor (Zaber, NA23C60-T4) with 60 mm travel range complemented with a pressure transducer (Gaeltec, CTN/4F-HP, Linearity: +-1%FS BSL, Sensitivity: 5µV/V/mmHg) was mounted opposite the specimen in the transversal plane of the IVD (figure 1B). The motor allowed to pull the pressure needle through the IVD in a well-controlled way to generate pressure profiles (figure 1C).

Biomechanical Test Protocol

The pressure profile of each specimen was recorded during axial compression loading with 400 N force and during the combined application of 7.5 Nm flexion or extension with 400 N axial compression. Prior to the first profilometry, the segments were preconditioned with 10 cycles of +/- 7.5 Nm flexion-extension. The pressure needle was manually inserted through the IVD until a pressure drop to zero clearly indicated that the transducer passed the dorsal annulus and the posterior longitudinal ligament. The pressure probe was oriented in the lateral direction to be less affected by the endplate (Adams et al., 1996). A custom-made Labview software (LabVIEW 2017) was used to record position and pressure during the retraction of the pressure needle with a sampling rate of 120 Hz and a constant velocity of 5 mm/s resulting in a special resolution of 24 values/mm. Testing was performed at room temperature with a humidity of about 50%. To prevent dehydration, the specimens were frequently sprayed with phosphate buffered saline (PBS). The same test sequence (neutral, flexion and extension) was applied for all specimens and loading duration was below one minute per test with a recovery time of about 2 minutes between tests.

Data analysis and statistical evaluation

Degeneration of the pressure profile has been associated with “deviation from a constant profile”, “increasing shorting of the constant part”, “H-shaped profiles”, “increasing numbers of peaks” and “discontinuity of the profile” (McNally et al., 1996). Mathematically, deviation from a constant profile can be described with the variance (or standard deviation) of the data and bumpiness or discontinuity

of the curve as the deviation from zero slope. The profile was normalized to the length of the pressure profile for independency of disc size and resampled to 100 data points to allow for better reproducibility of the method. The pressure amplitude was normalized to the mean pressure for independency of loading amplitudes. The pressure variation was formulated as

$$Pressure\ variation\ = std(\hat{p}_i) = \sqrt{\frac{1}{N-1}\sum_{i=1}^{N}(\hat{p}_i - \hat{\bar{p}})}$$

with $std = standard\ deviation$, $\hat{p}_i = normalized\ pressure$, $N = number\ of\ data\ points = 100$, $\hat{\bar{p}} = normalized\ mean\ pressure$ and $i = data\ point\ index$. Pressure discontinuity was defined as

$$Pressure\ discontinuity = mean\left(abs\left(\frac{\Delta\hat{p}_i}{\Delta\hat{l}}\right)\right) = \frac{1}{N}\sum_{i=1}^{N}\left|\frac{\Delta\hat{p}_i}{\Delta\hat{l}}\right|$$

with $abs = absolute\ value$ and $\frac{\Delta\hat{p}_i}{\Delta\hat{l}} = change\ in\ normalized\ pressure\ per\ normalized\ length.$

Since pressure variance and discontinuity were correlated ($\rho = 0.82$, $p < 0.001$), a principle component analysis (PCA) was performed to weigh to two components and to reduce on dimension. Principle component 1 was able to explain 99.94% of the variance. The pressure score was defined as

$$Pressure\ score = w_1 \times std(\hat{p}_i) + w_2 \times mean\left(abs\left(\frac{\Delta\hat{p}_i}{\Delta\hat{l}}\right)\right) = w_1 \times \sqrt{\frac{1}{N-1}\sum_{i=1}^{N}(\hat{p}_i - \hat{\bar{p}})} + w_2 \times \frac{1}{N}\sum_{i=1}^{N}\left|\frac{\Delta\hat{p}_i}{\Delta\hat{l}}\right|$$

with the weighing factor $w_1 = 0.0292$ and $w_2 = 0.9996$ as derived in the PCA.

The segmental pressure score was defined as the mean pressure scores recorded in flexion, extension and in the neutral position. To quantify the variability of the pressure profiles between these loading conditions, the average of the percental difference along the normalized profile for all combinations (flexion-extension, flexion-neutral, extension-neutral) was computed and a Spearman correlation rank test was preformed to test the relationship with the segmental pressure score. The relations between the segmental pressure score was evaluated with a Pearson correlation rank test and the radiological (Pfirrmann, Farshad, Rajasekaran) and the demographic parameters (age and BMI) were evaluated by

performing Spearman correlation rank tests. For the Rajasekaran system, the data were pooled in grade 1&2, grade 3&4 and grade 5&6. The specimens with any type of Modic change were grouped due to the small number for each individual type and the Mann-Whitney U test was used to evaluate the difference. Non-parametric testing was chosen since Shapiro-Wilk tests showed not all values to be normally distributed. Statistical significance was assumed with $p < 0.05$.

RESULTS

The segmental pressure scores ranged from 4 to 26.2 (figure 2) and were positively correlated with the percental profile difference (**rho = 0.81, p < 0.0001**) (figure 3).

From 39 specimens, 7 IVD were classified as Pfirrmann 2, 16 as Pfirrmann 3, 15 as Pfirrmann 4 and 1 as Pfirrmann 5. Median segmental pressure scores (interquartile distance) were 8.9 (6.1) for grade 2, 13.1 (19.5) for grade 3, 14.9 (6.3) for grade 3 and 22.7 (0) for grade 4. Segmental pressure score and Pfirrmann grade showed a significant positive correlation (**rho = 0.43, p = 0.006**) (figure 4).

8 segments were classified according to classification for segmental degeneration by Farshad (Farshad-Amacker et al., 2017) as 1, 29 as Farshad 2, and 2 as Farshad 3. Median pressure scores were 9.5 (7.1) for Farshad 1, 13.8 (7.8) for Farshad 2, and 19.4 (6.7) for Farshad 3. A significant positive correlation between segmental pressure score and the Farshad classification system was observed (**rho = 0.41, p = 0.009**) (figure 4).

The Rajasekaran endplate classification system separated the segments into 14 segments with Rajasekaran 1&2, 22 segments with Rajasekaran 3&4 and 3 segments with Rajasekaran 5&6 (mean value between cranial and caudal endplate). The segmental pressures scores were 12.3 (8.2) for Rajasekaran 1&2, 16.2 (6.2) for Rajasekaran 3&4, and 17.3 (5.0) for Rajasekaran 5&6. A significant positive correlation between segmental pressure score and the Rajasekaran grading was recorded (**rho = 0.39, p = 0.013**) (figure 4).

Modic changes were observed in 4 segments (3x Modic Type 2, 1x Modic Type 3) and were pooled together. The segmental pressure score was 12.3 (8.2) for the Modic group and 16.2 (6.2) for the non-Modic group. The difference did not reach statistical significance (p = 0.23) (figure 4).

Spearman correlation testing revealed a positive correlation between age and pressure score (rho = 0.32, p = 0.049) (figure 5). The association between BMI and pressure score (rho = -0.21, p = 0.201) was non-significant (figure 5).

DISCUSSION

The hydrostatic integrity of the intervertebral disc changes during the process of degeneration. Changes in the hydrostatic integrity of the disc create regional overload of the highly innervated endplates and are associated lower back pain (Jackson et al., 1966). Invasive pressure profiles would allow quantification of the hydrostatic integrity but are clinically not applicable as the procedure itself initiates disc degeneration. We aimed to find associations of MRI finding to invasive pressure profiles of IVDs to allow prediction of hydrostatic integrity by clinical MRI sequences. A novel pressure score was created to quantify the shape of the pressure profiles. The score showed significant associations to commonly used MRI gradings for disc-, endplate and segmental degeneration. More severe degenerative changes of the intervertebral disc (Pfirrmann classification) and the endplate (Rajasekaran classification) as well as segmental degeneration (Farshad classification) were correlated with higher pressure scores representing more irregular pressure profiles and reduced hydrostatic integrity. The estimation of the hydrostatic integrity of the IVD is therefore possible with the commonly applied grading systems based on clinical routine MRI sequences, however with limited correlation coefficients ranging from 0.39 to 0.43. The accuracy of this non-invasive method to evaluate the hydrostatic integrity of the intervertebral disc could be further increased with additional imaging approaches such as quantitative MRI, which could provide further information about compositional and structural characteristics of the intervertebral disc (Ellingson et al., 2014; Mwale et al., 2008; Nazari et al., 2015; Yamabe et al., 2017; Yang et al., 2020). However, the evaluation of these methods lies outside the scope of this manuscript.

Small pressure scores indicating a non-degenerated situation with intact hydrostatic integrity showed largely equal pressure profiles during the neutral, the flexed and extended loading condition. This observation indicates that the healthy IVD acts largely “waterbed”-alike and is able to distribute compressive loads uniformly, even when the segment is strongly bent. In specimens with higher pressure scores indicating hindered fluid dispersion, the difference between the three loading conditions was more distinct and in cases with very high pressure scores with completely

depressurized regions and regions with very high pressure amplitudes, a large variability between loading conditions was present.

The associations of the here observed degrees of degeneration and changes in hydrostatic integrity of the IVD can be used in the understanding of the process of segmental degeneration: In the healthy, non-degenerated spine, uniform load distribution is achieved thanks to the specific anatomy and composition of the IVD (figure 6). During early degeneration, a decrease in proteoglycans results in a reduced water content in the IVD (Boos et al., 2002) (especially in the nucleus), which impedes load distribution and results in an increasing fraction of the load being transmitted through the annulus (Adams and McNally, 1992; Adams and Roughley, 2006), which manifests in the H-shaped pressure profile (Przybyla et al., 2006). Such a load redistribution agrees with the observation, that in older subjects and in patients with more severe degree of degeneration, the trabecular structure and thickness are more developed in the peripheral regions of the vertebral body compared to the central region (Wang et al., 2013). According to Wolff's law, bone synthesis is highly sensitive to mechanical stimuli and increased force transmission through the peripheral region of the vertebra could cause such remodeling processes. Vice versa, less load is transmitted over the central region, in which the endplates were observed to become thinner (Roberts et al., 1997) and more porose with degeneration (Zehra et al., 2015). These changes could make them more susceptible to mechanical failure (Fields et al., 2010; Moore, 2006; Zehra et al., 2015; Zhao et al., 2009). Supporting this hypothesis, a decrease in proteoglycan content has been linked to reduced endplate thickness (Roberts et al., 1997). With further degeneration, the pressure profiles become increasingly irregular, indicating hindered pressure equalization. It has been hypothesized, that localized failure of the supporting endplates are causing such irregular loading patterns (Moore, 2000; Rade et al., 2017), since acute changes in pressure profiles could be induced by artificial endplate breakages (Przybyla et al., 2006). As a consequence of this hindered load equalization, localized overloading of the IVD could occur and initiate degenerative changes. This hypothesis is supported by the observation of cracks in the endplates in very young subjects (age 3-10 years) (Boos et al., 2002). However, irregular load distribution patterns could not only be caused by defects in the endplates, but also by structural changes of the IVD itself. The

increased load acting on the annulus (manifesting as the H-shaped pressure profile in early degeneration), could generate tears and internal annulus collapses, which can in turn initiate localized ossification (Adams and Roughley, 2006; Gunzburg et al., 1992). Such structural changes could impede pressure equalization, again resulting in localized pressure peaks, which could induce further tears and degeneration of the IVD and subsequent failure of the endplate in the area. The hypothesis of annulus tears as an initiating factor for the degenerative cascade is supported by the occurrence of tears in specimens without endplate failure (Senck et al., 2020). Based on these hypothesized pathomechanical processes, all initial lesions would consequently result in a combination of structural changes or defects of the IVD, weakened or defective endplate and reduced resilience of the vertebral body in the central region, combined with a highly irregular pressure distribution. This combination renders the segments vulnerable to painful endplate failure, disc herniation and progressive loss of disc height.

The current study is associated with several limitations. First, this study is based on cadaveric specimens, which were imaged without external loading (Kingma et al., 2000) and which were tested at room temperature. This could change the radiologic and biomechanical characteristics compared to the in-vivo situation, limiting direct transferability of the results to the clinical setting. Also, the applied loads cannot reflect the complex in-vivo loading conditions, which could cause different pressure distributions in the IVD. The test sequence was not varied, and the effect of long-time loading was not evaluated. The specifics of the applied methodology (e.g., temporal and spatial sampling rate, noise) could limit comparability of the results to pressure profiles measured by other groups, however the performed resampling of the data should help limit the effect of this aspect. The physical interpretation of the pressure profile is challenging. While the pressure profile in healthy specimens seems to adequately represent the hydrostatic pressure in the IVD, this relation is less clear with more erratic profiles. Pressure peaks might also result from solid structures in the IVD and not solely from fluid pressure (Adams and McNally, 1992). Nevertheless, the assumption that irregular pressure profiles indicate a non-uniform pressure distribution still appears reasonable. The conclusions are

based on measurements derived from a pressure profiles in the mid-sagittal plane. Even though similar pressure profiles can be expected in other regions, this assumption cannot be proven with our data.

A mathematical method was developed to quantify the shape of pressure profiles (pressure score). The pressure score correlates significantly with MRI gradings of the intervertebral disc (Pfirrmann), the endplate (Rajasekaran), the overall degenerative state of the spinal segments (Farshad) as well as age. It does not correlate with presence of Modic changes and BMI. These correlations show that an association between hydrostatic integrity of the IVD and the MRI appearance exists. However, the link is not very strong.

Acknowledgments

Imaging was performed with support of the Swiss Center for Musculoskeletal Imaging, SCMI, Balgrist Campus AG, Zürich, with special acknowledgement to Natalie Hinterholzer and Prof. Daniel Nanz. The authors gratefully acknowledge the contribution of Beda Rutishauser for his support with the mechanical test setup.

REFERENCES

Adams, M.A., McNally, D.S., 1992. Internal Intervertebral Disc Mechanics as Revealed by Stress Profilometry. Spine (Phila. Pa. 1976).

Adams, M.A., McNally, D.S., Dolan, P., 1996. “Stress” distributions inside intervertebral discs. J. Bone Jt. Surg. 78, 965–972. https://doi.org/10.1302/0301-620x78b6.1287

Adams, M.A., Roughley, P.J., 2006. What is intervertebral disc degeneration, and what causes it? Spine (Phila Pa 1976) 31, 2151–2161. https://doi.org/10.1097/01.brs.0000231761.73859.2c

Boos, N., Weissbach, S., Rohrbach, H., Weiler, C., Spratt, K.F., Nerlich, A.G., 2002. Classification of age-related changes in lumbar intervertebral discs: 2002 Volvo award in basic science. Spine (Phila. Pa. 1976). 27, 2631–2644. https://doi.org/10.1097/00007632-200212010-00002

Cornaz, F., Fasser, M.-R., Spirig, J.M., Snedeker, J.G., Farshad, M., Widmer, J., 2020. 3D printed clamps improve spine specimen fixation in biomechanical testing. J. Biomech. 98, 109467. https://doi.org/10.1016/j.jbiomech.2019.109467

Ellingson, A.M., Nagel, T.M., Polly, D.W., Ellermann, J., Nuckley, D.J., 2014. Quantitative T2* (T2 star) relaxation times predict site specific proteoglycan content and residual mechanics of the intervertebral disc throughout degeneration. J. Orthop. Res. 32, 1083–1089. https://doi.org/10.1002/jor.22633

Farshad-Amacker, N.A., Hughes, A., Herzog, R.J., Seifert, B., Farshad, M., 2017. The intervertebral disc, the endplates and the vertebral bone marrow as a unit in the process of degeneration. Eur. Radiol. 27, 2507–2520. https://doi.org/10.1007/s00330-016-4584-z

Fields, A.J., Lee, G.L., Keaveny, T.M., 2010. Mechanisms of initial endplate failure in the human vertebral body. J. Biomech. 43, 3126–3131. https://doi.org/10.1016/j.jbiomech.2010.08.002

Gruber, H., Rhyne, A., Hansen, K., Hoelscher, G., Ingram, J., Norton, H., Hanley, E., 2011. Deleterious Effects of Discography Radiocontrast Solution on Human Annulus Cells in Vitro: Changes in Cell Viability, Proliferation and Apoptosis in Exposed Cells. Spine J. 11, S41–S42. https://doi.org/10.1016/j.spinee.2011.08.110

Gunzburg, R., Parkinson, R., Moore, R., Cantraine, F., Hutton, W., Vernon-Roberts, B., Fraser, R., 1992. A Cadaveric Study Comparing Discography, Magnetic Resonance Imaging, Histology, and Mechanical Behavior of the Human Lumbar Disc. Spine (Phila. Pa. 1976). 17, 417–426.

https://doi.org/10.1097/00007632-199204000-00007

Jackson, H.C., Winkelmann, R.K., Bickel, W.H., 1966. Nerve endings in the human lumbar spinal column and related structures. J. Bone Joint Surg. Am. 48, 1272–1281. https://doi.org/10.2106/00004623-196648070-00002

Kingma, I., Van Dien, J.H., Nicolay, K., Maat, J.J., Weinans, H., 2000. Monitoring water content in deforming intervertebral disc tissue by finite element analysis of MRI data. Magn. Reson. Med. 44, 650–654. https://doi.org/10.1002/1522-2594(200010)44:4<650::AID-MRM21>3.0.CO;2-0

McNally, D.S., Adams, M.A., Goodship, A.E., 1992. Development and validation of a new transducer for intradiscal pressure measurement. J Biomed Eng 14, 495–498.

McNally, D.S., Shackleford, I.M., Goodship, A.E., Mulholland, R.C., 1996. In vivo stress measurement can predict pain on discography. Spine (Phila. Pa. 1976). https://doi.org/10.1097/00007632-199611150-00007

Modic, M.T., Steinberg, P.M., Ross, J.S., Masaryk, T.J., Carter, J.R., 1988. Degenerative disk disease: assessment of changes in vertebral body marrow with MR imaging. Radiology 166, 193–199. https://doi.org/10.1148/radiology.166.1.3336678

Moore, R.J., 2006. The vertebral endplate: Disc degeneration, disc regeneration. Eur. Spine J. 15, 333–337. https://doi.org/10.1007/s00586-006-0170-4

Moore, R.J., 2000. The vertebral end-plate: What do we know? Eur. Spine J. 9, 92–96. https://doi.org/10.1007/s005860050217

Mwale, F., Iatridis, J.C., Antoniou, J., 2008. Quantitative MRI as a diagnostic tool of intervertebral disc matrix composition and integrity. Eur. Spine J. 17, 432–440. https://doi.org/10.1007/s00586-008-0744-4

Nazari, J., Pope, M.H., Graveling, R.A., 2015. Feasibility of Magnetic resonance imaging (MRI) in obtaining nucleus pulposus (NP) water content with changing postures. Magn. Reson. Imaging 33, 459–464. https://doi.org/10.1016/j.mri.2015.01.006

Pfirrmann, C.W.A., Metzdorf, A., Zanetti, M., Hodler, J., Boos, N., 2001. Magnetic resonance classification of lumbar intervertebral disc degeneration. Spine (Phila. Pa. 1976). 26, 1873–1878. https://doi.org/10.1097/00007632-200109010-00011

Przybyla, A., Pollintine, P., Bedzinski, R., Adams, M.A., 2006. Outer annulus tears have less effect than

endplate fracture on stress distributions inside intervertebral discs: Relevance to disc degeneration. Clin. Biomech. 21, 1013–1019. https://doi.org/10.1016/j.clinbiomech.2006.07.003

Rade, M., Määttä, J.H., Freidin, M.B., Airaksinen, O., Karppinen, J., Williams, F.M., 2017. Vertebral Endplate Defect as Initiating Factor in Intervertebral Disc Degeneration; Strong Association between Endplate Defect and Disc Degeneration in the General Population. Spine (Phila. Pa. 1976). 43, 412–419. https://doi.org/10.1097/BRS.0000000000002352

Rajasekaran, S., Venkatadass, K., Naresh Babu, J., Ganesh, K., Shetty, A.P., 2008. Pharmacological enhancement of disc diffusion and differentiation of healthy, ageing and degenerated discs: Results from in-vivo serial post-contrast MRI studies in 365 human lumbar discs. Eur. Spine J. 17, 626–643. https://doi.org/10.1007/s00586-008-0645-6

Roberts, S., McCall, I.W., Menage, J., Haddaway, M.J., Eisenstein, S.M., 1997. Does the thickness of the vertebral subchondral bone reflect the composition of the intervertebral disc? Eur. Spine J. 6, 385–389. https://doi.org/10.1007/BF01834064

Senck, S., Trieb, K., Kastner, J., Hofstaetter, S.G., Lugmayr, H., Windisch, G., 2020. Visualization of intervertebral disc degeneration in a cadaveric human lumbar spine using microcomputed tomography. J. Anat. 236, 243–251. https://doi.org/10.1111/joa.13105

Wang, Y., Owoc, J.S., Boyd, S.K., Videman, T., Battié, M.C., 2013. Regional variations in trabecular architecture of the lumbar vertebra: Associations with age, disc degeneration and disc space narrowing. Bone 56, 249–254. https://doi.org/10.1016/j.bone.2013.06.022

Yamabe, D., Murakami, H., Chokan, K., Endo, H., Oikawa, R., Sawamura, S., Doita, M., 2017. Evaluation of Water Content in Lumbar Intervertebral Discs and Facet Joints before and after Physiological Loading Using T2 Mapping MRI. Spine (Phila. Pa. 1976). 42, E1423–E1428. https://doi.org/10.1097/BRS.0000000000002204

Yang, B., Wendland, M.F., O'Connell, G.D., 2020. Direct Quantification of Intervertebral Disc Water Content Using MRI. J. Magn. Reson. Imaging 52, 1152–1162. https://doi.org/10.1002/jmri.27171

Zehra, U., Robson-Brown, K., Adams, M.A., Dolan, P., 2015. Porosity and thickness of the vertebral endplate depend on local mechanical loading. Spine (Phila. Pa. 1976). 40, 1173–1180. https://doi.org/10.1097/BRS.0000000000000925

Zhao, F.D., Pollintine, P., Hole, B.D., Adams, M.A., Dolan, P., 2009. Vertebral fractures usually affect the cranial endplate because it is thinner and supported by less-dense trabecular bone. Bone 44, 372–379. https://doi.org/10.1016/j.bone.2008.10.048

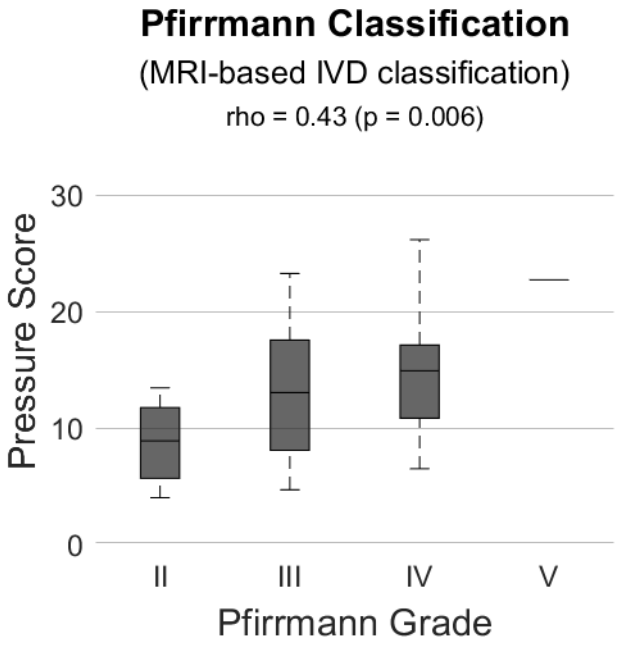

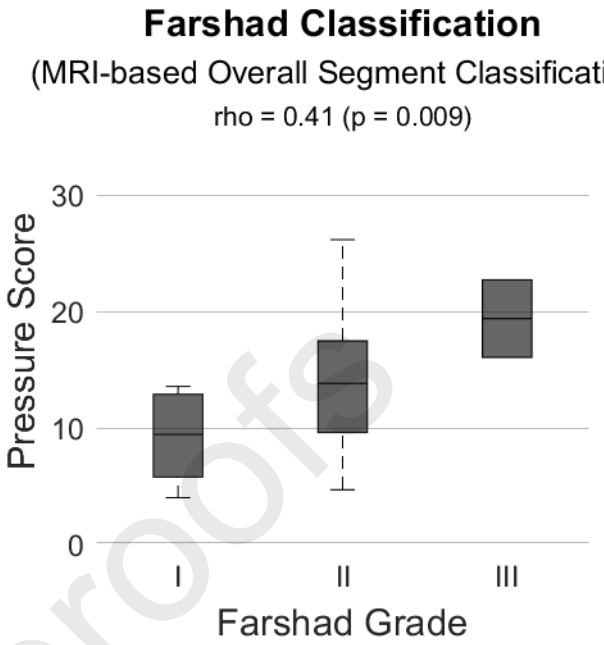

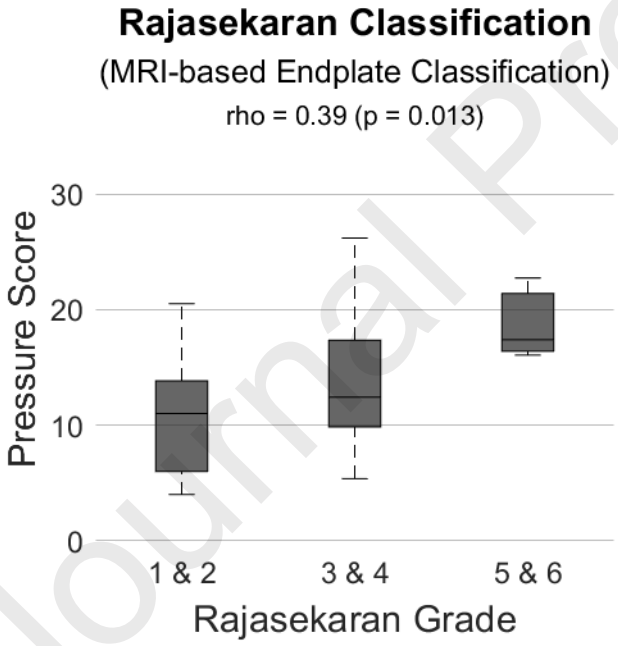

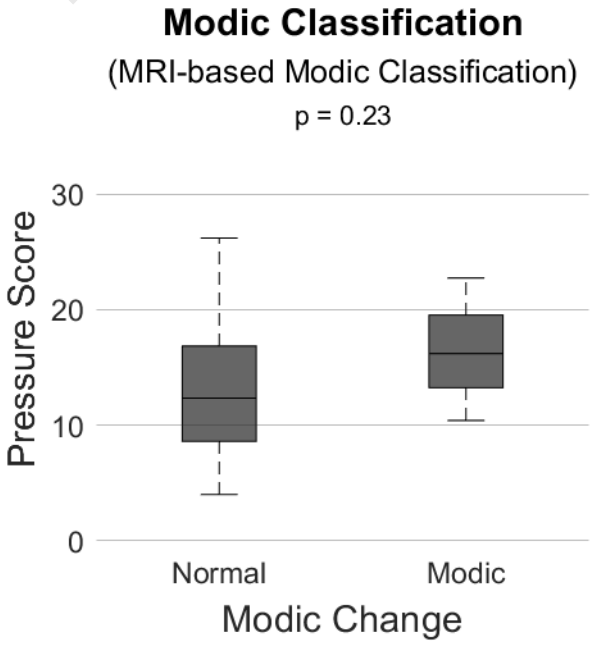

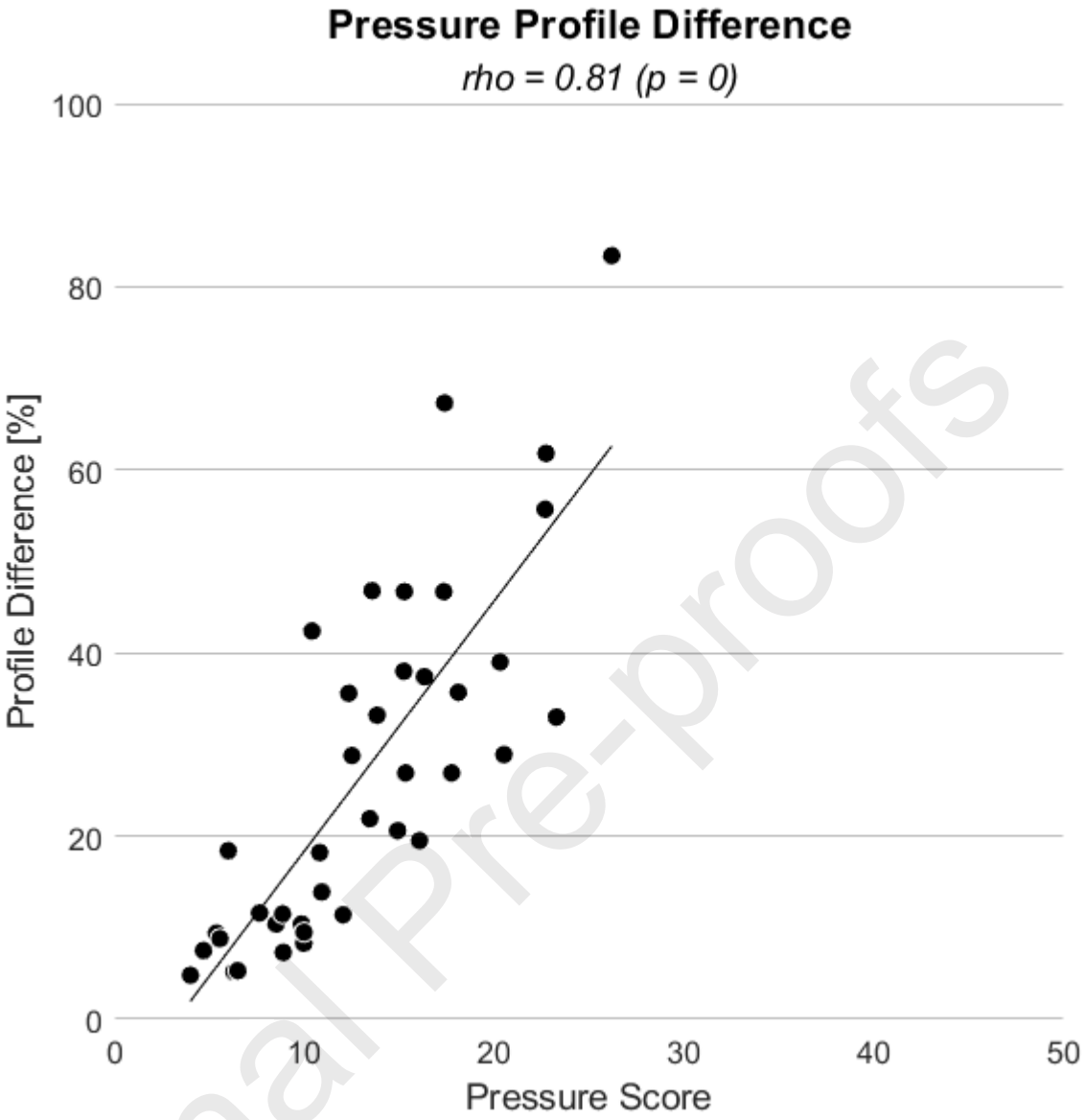

Pressure Profiles

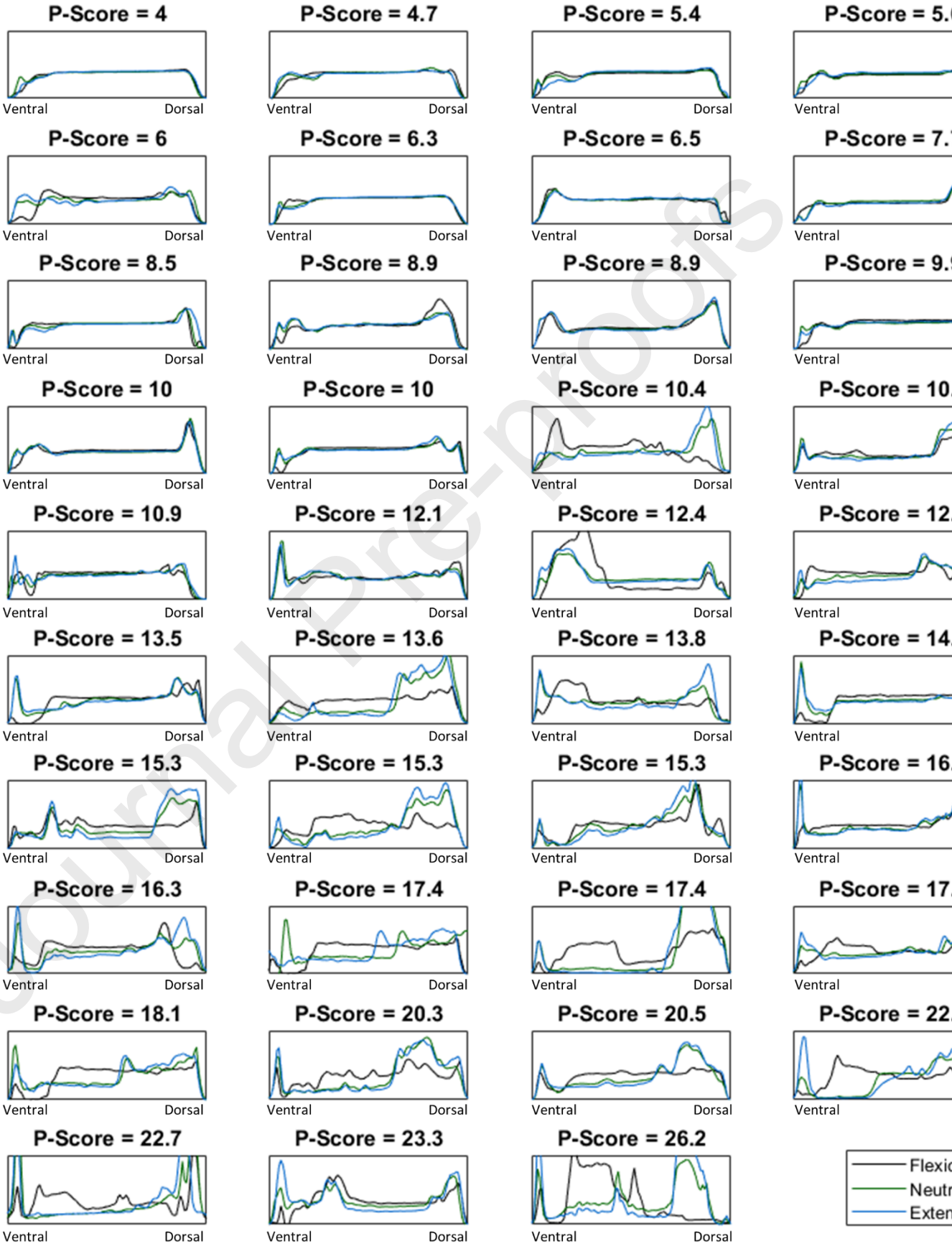

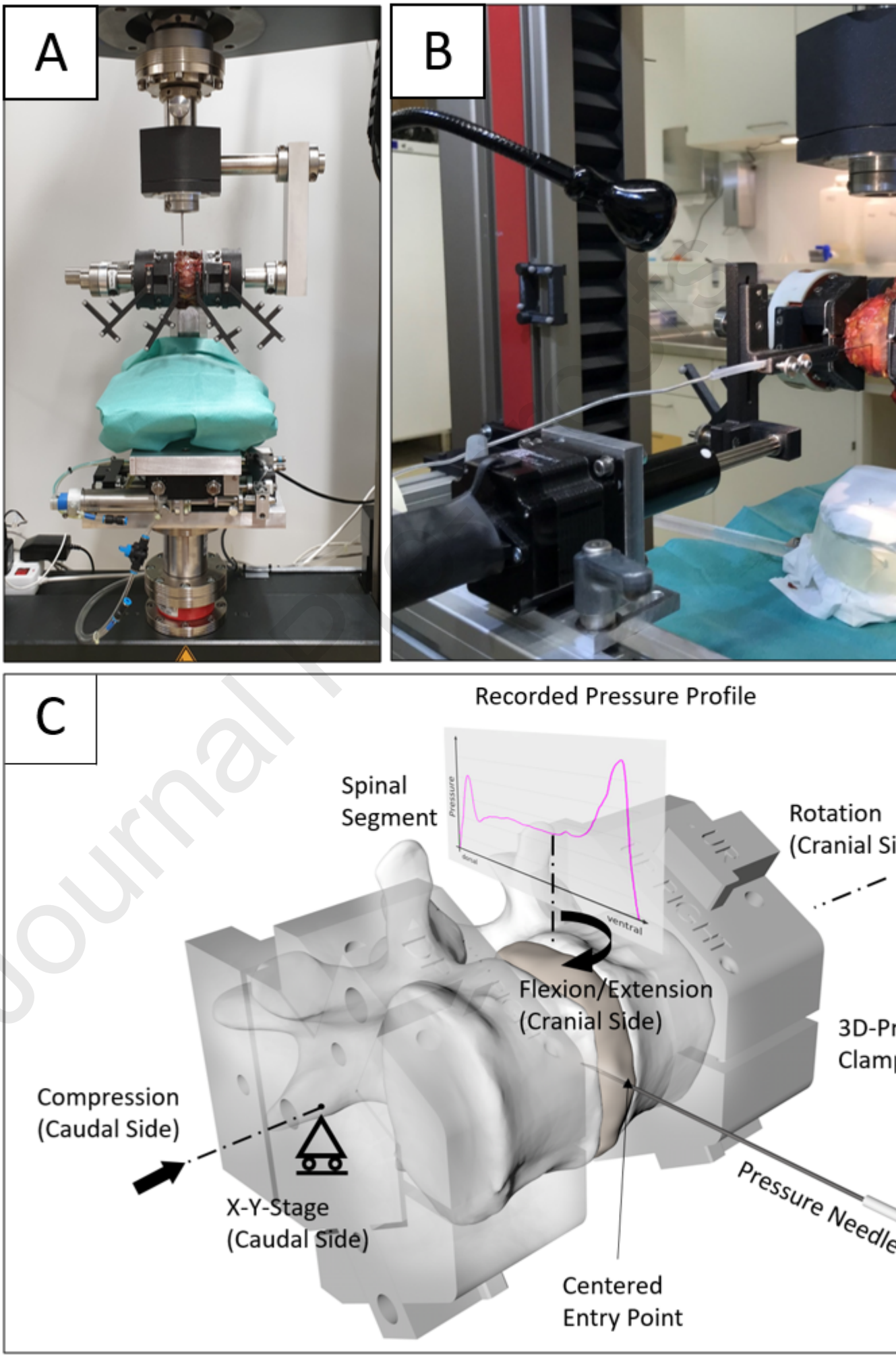
A
B
C
Recorded Pressure Profile
Spinal Segment
Pressure
dorsal
ventral
Rotation (Cranial Si
Flexion/Extension (Cranial Side)
3D-Pr
Clamp
Compression (Caudal Side)
X-Y-Stage (Caudal Side)
Pressure Needle
Centered Entry Point

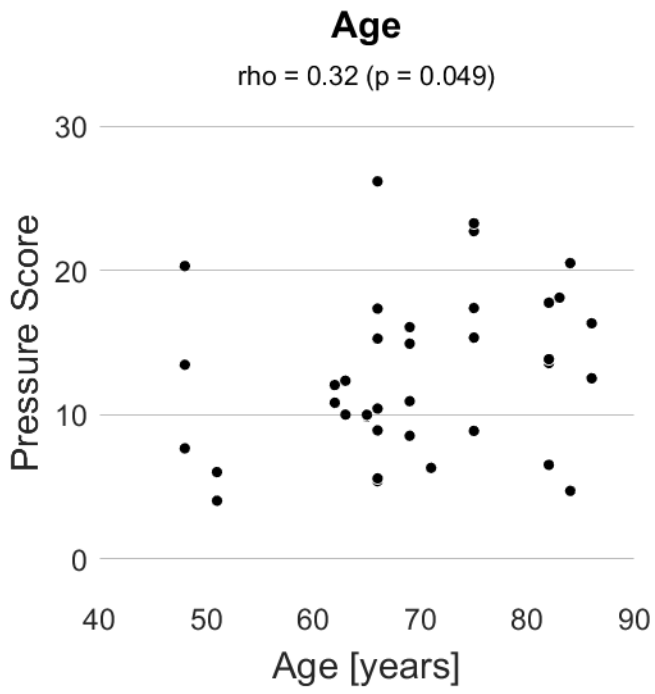

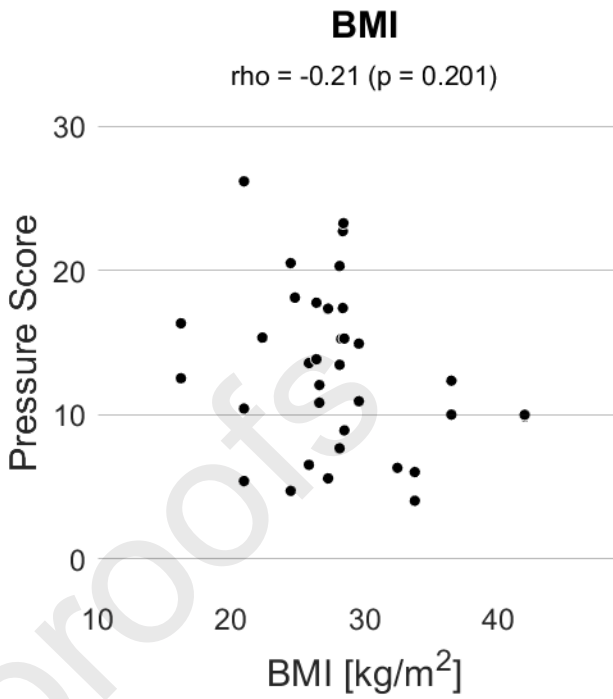

Figure 1: A) Spine testing setup for spinal segments. Axial compression can be combined with flexion and extension. B) The test rig including linear stepper motor and pressure needle. C) Schematic visualization of the experiment.

Figure 2: Mean pressure score (P-Score) from flexion, neutral and extension of 39 samples. The y-axis represents the normalized pressure and the x-axis represents the normalized position in the intervertebral disc from dorsal (left) to ventral (right).

Figure 3: Relation between the segmental pressure score and the profile difference. The profile difference was computed as mean percental difference between all three profiles (flexion, extension and neutral) compared to each other. The results of the Spearman correlation test are indicated, and a least-square line is fitted to illustrate the data distribution.

Figure 4: Association between segmental pressure score and radiologic grading systems (Pfirrmann, Farshad, Rajasekaran and Modic).

Figure 5: Correlation between segmental pressure score and demographic parameters (age and BMI).

Figure 6: Hydrostatic integrity and its role in the course of degeneration.

APPENDIX

Specimen	Level	P-Score (Mean)	P-Score (Flex.)	P-Score (Neutral)	P-Score (Ext.)	Pfirrmann	Farshad	Rajasekaran	Modic	Age	BMI
S182898	T12L1	4	3.7	4.7	3.7	2	1	2	1	51	33.8
S182571	L1L2	4.7	3.6	5.8	4.7	3	2	3	2	84	24.5
L181252	T12L1	5.4	6	5.7	4.5	3	2	5	2	66	21
S181915	T12L1	5.6	4.7	6.8	5.1	2	1	4	1	66	27.3
S182898	L4L5	6	5.4	6.6	6.1	2	1	3	1	51	33.8
S180106	L1L2	6.3	3.7	10	5.3	3	2	2	2	71	32.4
S180968	T12L1	6.5	7.4	7.1	5	4	2	7	2	82	25.8
S190353	T12L1	7.7	7.4	8	7.6	3	2	7	2	48	28.1
S180088	L1L2	8.5	7.4	10.6	7.6	3	2	6	2	69	50.1
S182576	T12L1	8.9	9.4	10.6	6.6	3	2	7	2	75	28.4
S181260	L1L2	8.9	7.6	10.1	9	2	1	4	1	66	28.5
S173430	L1L2	9.9	6.1	14.2	9.3	4	2	7	2	65	42
S173430	L3L4	10	7.6	16	6.3	3	2	5	2	65	42
S182575	L1L2	10	7.2	14.6	8.2	2	1	4	1	63	36.5
L181252	L4L5	10.4	9.9	11.6	9.7	4	2	5	2	66	21
S182452	L1L2	10.8	12.3	10.4	9.7	4	2	6	2	62	26.6
S180093	L1L2	10.9	10.2	11.1	11.5	4	2	5	2	69	29.6
S182452	L3L4	12.1	11.4	14	10.7	4	2	4	2	62	26.6
S182575	L3L4	12.4	10.8	15.6	10.6	2	1	5	1	63	36.5
L180769	L1L2	12.5	11.9	15.5	10.2	3	2	7	2	86	16.2
S190353	L4L5	13.5	10.8	16.7	12.9	2	1	3	1	48	28.1
S180968	L4L5	13.6	9	15.2	16.6	3	1	4	1	82	25.8
S181997	L3L4	13.8	9.8	17.7	14	4	2	4	2	82	26.4
S180093	L3L4	14.9	9.9	25.6	9.3	4	2	4	2	69	29.6
S181221	L4L5	15.3	12.3	16.4	17.1	3	2	5	2	66	28.2
S181260	L3L4	15.3	8.5	21.6	15.7	3	2	5	2	66	28.5
S181934	T12L1	15.3	13.8	15	17.2	4	2	5	2	75	22.3
S180088	L3L4	16.1	11.8	19.1	17.3	4	3	8	3	69	50.1
L180769	L3L4	16.3	12	16.4	20.6	4	2	7	2	86	16.2
S181915	L2L3	17.4	7.1	30.6	14.4	3	2	8	2	66	27.3
S182664	T12L1	17.4	14.1	19.1	19	4	2	10	2	75	28.4
S181997	L1L2	17.8	16.8	20.8	15.6	3	2	4	2	82	26.4
S181890	L4L5	18.1	8.6	29	16.8	4	2	6	2	83	24.8
S190353	L2L3	20.3	17.4	23.4	20.2	3	2	7	2	48	28.1
S182571	L3L4	20.5	11.1	37	13.5	4	2	4	2	84	24.5
S182664	L4L5	22.7	23.5	21.9	22.7	3	2	7	2	75	28.4
S182664	L2L3	22.7	10.6	25.2	32.4	5	3	12	3	75	28.4
S182576	L4L5	23.3	22.5	28.7	18.7	3	2	8	2	75	28.4
L181252	L2L3	26.2	20.9	28.8	28.9	4	2	5	2	66	21